72-76 Valence Electron Clusters: An Extension of the 16-18 Electron Rule. Synthesis, Crystal Structure, and Solution Dynamics of the Trigonal-Bipyramidal Pentanuclear Clusters $[PtIr_4(CO)_9(\mu\text{-}CO)_5]^{2-}$ and $[PtIr_4(CO)_9(\mu\text{-}CO)_3]^{2-}$

Alessandro Fumagalli,*[1a] Roberto Della Pergola,[1b] Fabio Bonacina,[1b] Luigi Garlaschelli,[1b] Massimo Moret,[1c] and Angelo Sironi*[1c]

Contribution from C.N.R., Centro di Studio per la Sintesi e la Struttura dei Composti dei Metalli di Transizione nei Bassi Stati di Ossidazione, Dipartimento di Chimica Inorganica e Metallorganica, Università di Milano, and Istituto di Chimica Strutturistica Inorganica, Università di Milano, Via G. Venezian 21, 20133 Milano, Italy. *Received April 25, 1988*

Abstract: The 76 CVE (cluster valence electron) species $[PtIr_4(CO)_{14}]^{2-}$ (**1**), obtained by the reductive carbonylation of a mixture of Na_2PtCl_6 and $IrCl_3 \cdot xH_2O$ or $Ir_4(CO)_{12}$, is in equilibrium with the 72 CVE species $[PtIr_4(CO)_{12}]^{2-}$ (**2**) through the dissociation-association of two carbonyl ligands. Both anions were characterized by the single-crystal X-ray diffraction of their respective $[PPh_4]^+$ and $[NEt_4]^+$ salts. $[PPh_4]_2[PtIr_4(CO)_{14}]$ crystallizes in the space group $P\bar{1}$ with $Z = 2$, $a = 13.868$ (3) Å, $b = 21.997$ (5) Å, $c = 10.804$ (2) Å, $\alpha = 102.51$ (2)°, $\beta = 106.29$ (2)°, $\gamma = 98.02$ (2)°. Some $[Ir_6(CO)_{15}]^{2-}$ (ca. 10%) was found cocrystallized in the cell. The structure was solved and refined to $R = 0.033$ and $R_w = 0.039$ for 6545 independent reflections with $I > 3\sigma(I)$. $[NEt_4]_2[PtIr_4(CO)_{12}]$ crystallizes in the orthorhombic space group *Pnma* (nonstandard setting of *Pnam*, *n*.62) with $Z = 12$, $a = 15.453$ (5) Å, $b = 22.340$ (5) Å, $c = 33.422$ (8) Å. The structure was solved and refined to $R = 0.056$ and $R_w = 0.057$ for 1579 independent reflections with $I > 3\sigma(I)$. Both anions have a trigonal-bipyramidal frame, the Pt atom in **1** being equatorial and in **2** apical. In **1**, where the ideal symmetry is C_2, nine carbonyls are terminally bonded (three on each apical Ir atom and one on each of the other metals), and five span the equatorial metal triangle and two opposite Ir_{eq}-Ir_{ap} edges. In **2**, with ideal C_s symmetry, nine carbonyls are terminally bonded (two on each of the Ir atoms and one on Pt), while the remaining three span one Ir_{eq}-Ir_{ap} and two Ir_{eq}-Pt edges. The ligand disposition on the apical metals, considering an additional ideal direction as that pointing toward the central triangle, appears trigonal bipyramidal in **1** and square planar in **2**, representative of saturated 18-electron and unsaturated 16-electron configurations, respectively. ^{13}C and ^{195}Pt NMR showed temperature dependent fluxional behavior of the COs in both anions.

Pentanuclear carbonyl clusters with a trigonal-bipyramidal metal frame occur with both 72 or 76 CVEs (cluster valence electrons); the former case is quite uncommon, there being only two osmium clusters, $Os_5(CO)_{16}$ and $[HOs_5(CO)_{15}]^-$,[2] and the recently reported $Ru_5(CO)_6(\eta\text{-}C_5H_5)_4$.[3]

They are generally mono- or dianions and attain the proper electronic configuration with a variable number of carbonyl ligands, up to a maximum of 16. Recent work has shown that it is possible to synthesize selectively mono- or bimetallic clusters of this kind; the compounds, for the most part containing rhodium, are of a general formula $[MRh_4(CO)_x]^{y-}$, with M = Fe,[4] Ru,[5] Os[6] ($x = 15$, $y = 2$), Rh,[7] Ir[8] ($x = 15$, $y = 1$), Pt[9] ($x = 12$, 14; $y = 2$). Most of the clusters of this family appear only in the form with 76 CVEs, generally stabilized by a carbon monoxide atmosphere. Under nitrogen, they decompose fairly easily, often irreversibly yielding species of higher nuclearity; only the $[PtRh_4(CO)_{14}]^{2-}$ was found to reversibly lose CO to give the related dianion $[PtRh_4(CO)_{12}]^{2-}$.

After the isolation of $[MIr_4(CO)_{15}]^{2-}$ (M = Fe,[10] Ru[11]) and while searching for other similar species containing an Ir_4 moiety, we synthesized the presently reported $[PtIr_4(CO)_{14}]^{2-}$ which, like the analogous Pt-Rh species, gives, by the dissociation of two carbonyl ligands, a related species, $[PtIr_4(CO)_{12}]^{2-}$. This case, reported here with a full crystallographic analysis, is the only other example of facile interconversion between the two forms known with 76 and 72 CVEs respectively, for trigonal bipyramidal clusters.

Results and Discussion

Synthesis and Reactivity of $[PtIr_4(CO)_{14}]^{2-}$ and $[PtIr_4(CO)_{12}]^{2-}$. The choice to use reductive carbonylation for the synthesis of $[PtIr_4(CO)_{14}]^{2-}$ was made on the basis of our previous experience, which indicated pentanuclear dianionic clusters as species stable under CO atmosphere, even in strongly reducing conditions.[5,6,9-11] Thus Na_2PtCl_6 and hydrated $IrCl_3$, 1:4 molar ratio in methanolic solution, are reduced at room temperature and under 1 atm of carbon monoxide, by adding NaOH, usually in slight excess over the stoichiometry of eq 1. The intermediate equilibrations of this

$$[PtCl_6]^{2-} + 4IrCl_3 + 27OH^- + 23CO \rightarrow [PtIr_4(CO)_{14}]^{2-} + 18Cl^- + 9H_2O + 9HCO_3^- \quad (I)$$

multistep reduction are not as ready as they are in the virtually identical reduction of the Na_2PtCl_6 and $RhCl_3$ mixture which yields the analogous $[PtRh_4(CO)_{14}]^{2-}$, and the overall reaction is slower. According to IR monitoring of the reduction, after an induction time of 1-2 h, the first carbonylic species observed is an unidentified carbonyl of iridium with an IR absorption at 1965 cm^{-1}; the red-brown solution subsequently becomes cloudy due to the precipitation of NaCl, and at the same time, the formation of $[Ir(CO)_4]^-$[12] along with $[Pt_9(CO)_{18}]^{2-}$,[13] is observed, with no clear evidence of intermediate products. The mixed species $[PtIr_4(CO)_{14}]^{2-}$ gradually increases in concentration as the two homonuclear species decrease. It is worth mentioning that the intermediate mixed species $[PtRh_5(CO)_{15}]^-$[9] was observed in the

(1) (a) CNR. (b) Dipartimento di Chimica Inorganica e Metallorganica. (c) Istituto di Chimica Strutturistica Inorganica.
(2) (a) Eady, C. R.; Johnson, B. F. G.; Lewis, J.; Reichert, B. E.; Sheldrick, G. M. *J. Chem. Soc., Chem. Commun.* **1976**, 271. (b) Guy, J. J.; Sheldrick, G. M. *Acta Crystallogr., Sect. B* **1978**, *34*, 1722.
(3) Knox, S. A. R.; Morris, M. J. *J. Chem. Soc., Dalton Trans.* **1987**, 2087.
(4) Ceriotti, A.; Longoni, G.; Della Pergola, R.; Heaton, B. T.; Smith, D. O. *J. Chem. Soc., Dalton Trans.* **1983**, 1433.
(5) Fumagalli, A.; Ciani, G. *J. Organomet. Chem.* **1984**, *272*, 91.
(6) Fumagalli, A.; Garlaschelli, L.; Della Pergola, R. *J. Organomet. Chem.*, in press.
(7) Fumagalli, A.; Koetzle, T. F.; Takusagawa, F.; Chini, P.; Martinengo, S.; Heaton, B. T. *J. Am. Chem. Soc.* **1980**, *102*, 1740.
(8) Della Pergola, R. *XIX Congresso Nazionale di Chimica Inorganica*, Oct 6-10, 1986, Università di Cagliari, Abs. A53.
(9) Fumagalli, A.; Martinengo, S.; Chini, P.; Galli, D.; Heaton, B. T.; Della Pergola, R. *Inorg. Chem.* **1984**, *23*, 2947.
(10) Della Pergola, R.; Garlaschelli, L.; Demartin, F.; Manassero, M.; Masciocchi, N.; Sansoni, M.; Fumagalli, A. *J. Chem. Soc., Dalton Trans.*, in press.
(11) Fumagalli, A.; Koetzle, T. F.; Takusagawa, F. *J. Organomet. Chem.* **1981**, *213*, 365.

0002-7863/89/1511-0165$01.50/0

Table I. IR Data[a]

compd	cation	solvent	CO stretchings										
$[PtIr_4(CO)_{14}]^{2-}$	Na	MeOH	2016 s	1972 vs	1950 sh	1915 mw	1820 mw	1805 mw	1790 mw	1755 mw			
	N-*n*-Bu_4	THF	2040 w	2006 s	1987 m	1965 sh	1960 vs	1850 w	1816 sh	1808 m	1784 m	1770 m	1715 m
	NMe-*n*-Bu_3	THF	2039 w	2007 s	1989 m	1966 sh	1960 vs	1852 w	1808 m	1784 m	1774 m	1706 m	
	PPN	THF	2035 w	2000 s	1980 m	1963 sh	1956 vs	1934 m	1814 m	1782 m	1721 m		
	PPN	MeCN	2042 w	2011 s	1988 sh	1963 vs	1943 m	1811 m	1778 m	1717 m			
$[PtIr_4(CO)_{12}]^{2-}$	N-*n*-Bu_4	THF	2025 w	1979 vs	1940 ms	1915 w	1782 m	1750 m					
	NMe-*n*-Bu_3	THF	2025 w	1975 vs	1940 ms	1915 w	1780 m	1750 m					
	PPN	THF	2024 w	1975 vs	1939 ms	1914 w	1775 sh	1765 m					
	PPN	MeCN	2031 w	1983 vs	1945 ms	1925 sh	1770 sh	1763 m					

[a] Wavenumbers are in cm^{-1} (± 2 cm^{-1}): vs = very strong, s = strong, m = medium, w = weak, sh = shoulder.

reductive sequence of Na_2PtCl_6 and $RhCl_3 \cdot xH_2O$, and, in fact, $[PtRh_4(CO)_{14}]^{2-}$ was found to originate from the reduction of this hexanuclear species. No intermediate bimetallic species was evident in the present case. The reaction is complete within 18–24 h when an orange-brown solution is formed.

Alternatively the product can be obtained by reducing $Ir_4(CO)_{12}$ and Na_2PtCl_6; this modification has the advantage of a cleaner reaction and slightly better yields. The course of the reduction is different. Due to the high initial concentration of NaOH, reduction of Na_2PtCl_6 to $[Pt_9(CO)_{18}]^{2-}$ occurs quite rapidly, while the insoluble $Ir_4(CO)_{12}$ reacts slowly to give at first a compound which, from the IR spectrum, seems to be $[Ir_4(CO)_{11}COOMe]^-$,[14] and which subsequently becomes $[Ir_4(CO)_{11}H]^-$.[15] $[Ir(CO)_4]^-$ is not evident at any time. From this point on, condensation, to give the mixed pentanuclear dianion, is observed.

Upon standing the reaction medium becomes less and less reducing because, in the presence of carbon monoxide, the hydroxide anion gives formate, as previously observed in a reaction which is apparently catalyzed by iridium carbonyl anions.[16] In this condition the formation of $[Ir_6(CO)_{15}]^{2-}$[17] is favored, an undesirable result which is usually without remedy since the stability of this anion is such that it cannot be recycled to give back the mixed species, even if strongly reducing conditions are restored. At this point, due to the similar solubility of the two anions, the recovering of pure $[PtIr_4(CO)_{14}]^{2-}$ can become arduous if not impossible. Thus some $[PPh_4]_2[Ir_6(CO)_{15}]$ (ca. 10%) was found cocrystallized with $[PPh_4]_2[PtIr_4(CO)_{14}]$ (vide infra). For these reasons it is therefore advisable to recover the product by precipitation with a chosen bulky cation as soon as possible.

The isolated, pure $[PtIr_4(CO)_{14}]^{2-}$ dianion is canary yellow, and, while it appears indefinitely stable under carbon monoxide, in nitrogen atmosphere there is a color change to red-brown. This process, seen both in solution and on the finely powdered solid, is due to the loss of carbon monoxide and is faster under vacuum where a gradual conversion to the related $[PtIr_4(CO)_{12}]^{2-}$ is obtained. These two species appear to be in reversible equilibrium, through the dissociation and association of two carbonyl ligands, according to eq 2. In the presence of CO at ca. 1 atm, from room

$$[PtIr_4(CO)_{14}]^{2-} \rightleftarrows [PtIr_4(CO)_{12}]^{2-} + 2CO \qquad (2)$$

temperature down to ca. −90 °C, we had spectroscopic evidence only of the species at the left, and, in fact, only this is recovered by precipitation. However, a few cycles of evacuation to dryness followed by redissolution in THF or acetone eventually result in a complete conversion to $[PtIr_4(CO)_{12}]^{2-}$. During this process, where the two anions coexist, there is no evidence of an intermediate step corresponding perhaps to the dissociation of a single CO. The red-brown $[PtIr_4(CO)_{12}]^{2-}$ is very reactive and, as revealed by ^{13}C and ^{195}Pt NMR, minimal traces of CO, perhaps

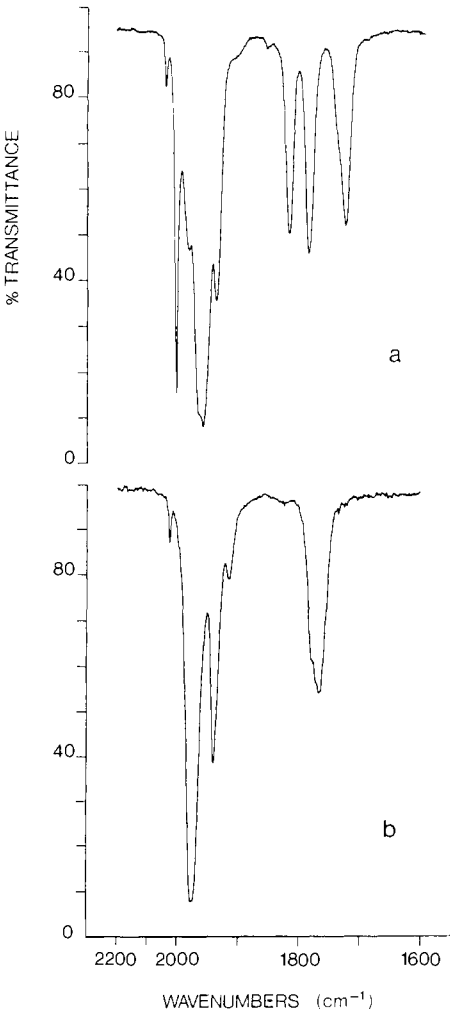

Figure 1. IR spectra in THF of the PPN salts of (a) $[PtIr_4(CO)_{14}]^{2-}$ and (b) $[PtIr_4(CO)_{12}]^{2-}$.

generated from a partial decomposition, immediately restore $[PtIr_4(CO)_{14}]^{2-}$.

All the bulky cation salts of $[PtIr_4(CO)_{14}]^{2-}$ must be handled and stored under CO atmosphere; they are soluble in THF, acetone and acetonitrile, sparingly soluble in MeOH, and insoluble in 2-propanol; the red-brown salts of the $[PtIr_4(CO)_{12}]^{2-}$ dianion are all soluble in acetone and acetonitrile, moderately soluble in THF (less than the corresponding salts of $[PtIr_4(CO)_{14}]^{2-}$), and insoluble in MeOH and 2-propanol. Both anions are very reactive with air even as solids, particularly $[PtIr_4(CO)_{12}]^{2-}$ which, in solution, is not very stable even under nitrogen and in a few days can decompose to yield $[Ir_6(CO)_{15}]^{2-}$ and other uncharacterized species.

IR Spectra. Reference IR spectra of both anions as PPN[18] salts in THF solution are reported in Figure 1. A noticeable dependence upon the cation and/or the solvent was observed (Table

(12) Garlaschelli, L.; Chini, P.; Martinengo, S.; *Gazz. Chim. Ital.* **1982**, *112*, 285.
(13) Longoni, G.; Chini, P. *J. Am. Chem. Soc.* **1976**, *98*, 7225.
(14) Garlaschelli, L.; Martinengo, S.; Chini, P.; Canziani, F.; Bau, R. *J. Organomet. Chem.* **1981**, *213*, 379.
(15) Bau, R.; Chiang, M. Y.; Wei, C. Y.; Garlaschelli, L.; Martinengo, S.; Koetzle, T. F. *Inorg. Chem.* **1984**, *23*, 4758.
(16) Angoletta, M.; Malatesta, L.; Caglio, G. *J. Organomet. Chem.* **1975**, *94*, 99.
(17) Demartin, F.; Manassero, M.; Sansoni, M.; Garlaschelli, L.; Martinengo, S.; Canziani, F. *J. Chem. Soc., Chem. Commun.* **1980**, 903.

(18) [PPN] = bis(triphenylphosphine)iminium cation.

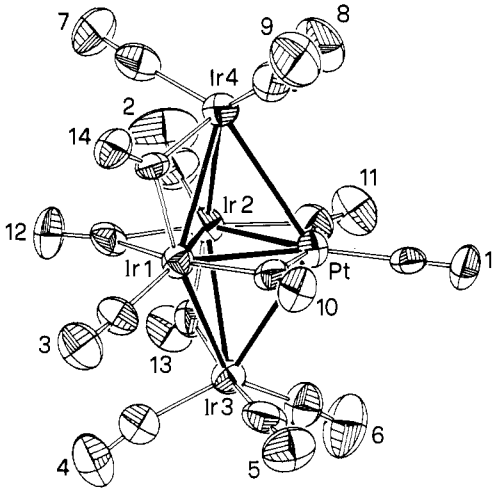

Figure 2. ORTEP drawing of $[PtIr_4(CO)_{14}]^{2-}$ anion. Carbon atoms of the CO groups bear the same numbering as the oxygen atoms.

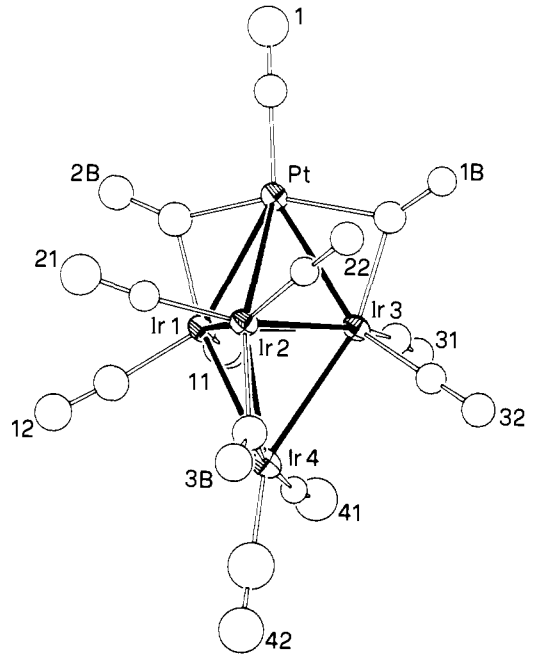

Figure 3. ORTEP drawing of $[PtIr_4(CO)_{12}]^{2-}$ anion. Carbon atoms of the CO groups bear the same numbering as the oxygen atoms.

I), probably due to ion pairing effects. The IR spectra of $[PtIr_4(CO)_{14}]^{2-}$, recorded under 1 atm of CO, are very similar in the shape and relative intensities of the bands to those of other pentanuclear clusters, particularly $[PtRh_4(CO)_{14}]^{2-}$; this is due to close structural features (vide infra). The IR spectra of $[PtIr_4(CO)_{12}]^{2-}$, are strongly modified and the two bands due to the terminal COs are shifted to lower wavenumbers of ca. 25 cm^{-1}. This is consistent with the loss of ligands and the consequent increased back-donation toward the remaining COs.

Description of the Structures of $[PtIr_4(CO)_{14}]^{2-}$ and $[PtIr_4(CO)_{12}]^{2-}$. The structures of the two anions are reported as ORTEP drawings in Figures 2 and 3. Selected bond distances for the two clusters are given in Tables II and III.

Both $[PtIr_4(CO)_{14}]^{2-}$ (**1**) and $[PtIr_4(CO)_{12}]^{2-}$ (**2**) have distorted trigonal bipyramidal cores with the Pt atom in equatorial and apical position, respectively. The position of platinum, inferred from the local ligand stereochemistry and confirmed by ^{13}C and ^{195}Pt NMR (vide infra), is the same as previously found in the closely related $[PtRh_4(CO)_{14}]^{2-}$ and $[PtRh_4(CO)_{12}]^{2-}$ anions.[9] The trigonal bipyramid of **1**, with average $M_{ap}-M_{eq}$ and $M_{eq}-M_{eq}$ distances of 3.062 and 2.702 Å, is rather elongated, as is usually found in this type of 76 CVE species. In **2** the corresponding average values, 2.826 and 2.740 Å, are consistent with the expected

Table II. Bond Distances (Å) for **1**

Pt–Ir1	2.697 (1)		
Pt–Ir2	2.692 (1)		
Pt–Ir3	3.106 (1)		
Pt–Ir4	3.165 (1)		
Ir1–Ir2	2.718 (1)		
Ir1–Ir3	3.062 (1)		
Ir1–Ir4	3.007 (1)		
Ir2–Ir3	2.987 (1)		
Ir2–Ir4	3.044 (1)		
Pt–C1	1.87 (1)	C1–O1	1.11 (1)
Ir1–C3	1.84 (1)	C3–O3	1.13 (1)
Ir2–C2	1.88 (1)	C2–O2	1.12 (1)
Ir3–C4	1.93 (1)	C4–O4	1.12 (1)
Ir3–C5	1.93 (1)	C5–O5	1.13 (1)
Ir3–C6	1.92 (1)	C6–O6	1.12 (1)
Ir4–C7	1.96 (1)	C7–O7	1.10 (1)
Ir4–C8	1.97 (1)	C8–O8	1.07 (1)
Ir4–C9	1.89 (1)	C9–O9	1.12 (1)
Pt–C10	2.14 (1)	C10–O10	1.18 (1)
Ir1–C10	2.07 (1)		
Pt–C11	2.15 (1)	C11–O11	1.15 (1)
Ir2–C11	2.11 (1)		
Ir1–C12	2.14 (1)	C12–O12	1.15 (1)
Ir2–C12	2.10 (1)		
Ir2–C13	2.06 (1)	C13–O13	1.16 (1)
Ir3–C13	2.07 (1)		
Ir1–C14	2.01 (1)	C14–O14	1.17 (1)
Ir4–C14	2.10 (1)		

Table III. Bond Distances (Å) for **2**

Pt–Ir1	2.701 (4)		
Pt–Ir2	3.024 (4)		
Pt–Ir3	2.709 (5)		
Ir1—Ir2	2.716 (4)		
Ir1–Ir3	2.794 (5)		
Ir1–Ir4	2.870 (4)		
Ir2–Ir3	2.712 (5)		
Ir2–Ir4	2.780 (5)		
Ir3–Ir4	2.871 (4)		
Pt–C1	1.81 (6)	C1–O1	1.15 (4)
Ir1–C11	1.89 (6)	C11–O11	1.14 (5)
Ir1–C12	1.84 (6)	C12–O12	1.13 (5)
Ir2–C21	1.81 (6)	C21–O21	1.16 (5)
Ir2–C22	1.81 (5)	C22–O22	1.16 (4)
Ir3–C31	1.79 (6)	C31–O31	1.15 (5)
Ir3–C32	1.85 (5)	C32–O32	1.15 (4)
Ir4–C41	1.82 (5)	C41–O41	1.20 (5)
Ir4–C42	1.81 (6)	C42–O42	1.15 (5)
Pt–C1B	2.02 (7)	C1B–O1B	1.26 (4)
Ir3–C1B	1.95 (7)		
Pt–C2B	1.82 (7)	C2B–O2B	1.22 (5)
Ir1–C2B	1.97 (8)		
Ir2–C3B	1.97 (8)	C3B–O3B	1.20 (5)
Ir4–C3B	1.97 (7)		

more regular metal skeleton of the 72 CVE species. These average values, particularly for $M_{ap}-M_{eq}$, arise from bond lengths which are rather scattered because of distortions in both anions. These irregularities can be classified as follows: (i) CO bridged edges are shorter than the corresponding unbridged ones; this is particularly evident in **2**, where this implies two off-center capping atoms; Pt with two short (av 2.705 Å) against one rather elongated (3.024 Å) Pt–Ir bonds and Ir4 with two long (av 2.870 Å) against one shorter (2.780 Å) Ir–Ir bond. (ii) CO bridged Pt–Ir bonds are shorter than corresponding bridged Ir–Ir (av 2.695 vs 2.718 in **1** and av 2.705 vs 2.780 Å in **2**). (iii) Unbridged Pt–Ir bonds are longer than corresponding unbridged Ir–Ir (av 3.136 vs av 3.053 Å in **1** and 3.024 vs av 2.871 Å).

The idealized symmetry in **1** is C_2 with the 2-fold axis passing through the equatorial Pt atom and bisecting the Ir1–Ir2 edge; the nine terminal carbonyls are three on each of the apical iridium atoms and one on each of the other metals. The bridging COs

Table IV. Variable Temperature ^{13}C NMR Spectra of $[PtIr_4(CO)_{14}]^{2-}$ as $[N\text{-}n\text{-}Bu_4]^+$ salt in THF-d_8 (δ in ppm)[a]

	room temp	−10 °C	−50 °C	−97 °C	(I), −97 °C	(II), −105 °C
C1	207.1 (2381.5)	207.2 (2382)	207.2 (2379)	207.4 (2380)	206.8 (2377)	193.2 (2250)
C2	196.5 [91.8]	196.5 [89.7]	196.6 [86.5]	196.7 [87]	196.0 [87]	205.9
C3	225.7 (481) {24}	226.1 (482) {25.5}	226.4 (485) {27.2}	226.9 (487) {25.6}	227.1 (484) {ca. 24}	245.5 (654)
C4	235.9 {ca. 25}	236.1 {25.5}	236.1 {23.9}	236.0 {25.5}	236.1 {25.4}	256.6
C5	215.9	215.9	216.0 {collps}	216.1 {27.6}	215.6 {26.9}	247.4
C6, 7, 8	177.9	C6	174.6 {ca. 27}	174.9 {27.5}	174.0 {27.6}	197.5
		C7	178.5	178.6	177.8	199.9
		C8	181.0	181.0	180.2	207.7

[a] Comparison with the $[PPN]^+$ salt (I) in acetone-d_6 at −97 °C and $[N\text{-}n\text{-}Bu_4]_2[PtRh_4(CO)_{14}]$ (II) in THF-d_8 at −105 °C.[9] ($^1J_{Pt-C}$), [$^2J_{Pt-C}$], and {$^2J_{C-C}$} are given ±1 Hz for ^{13}C and ±3.5 Hz for ^{195}Pt.

Chart I

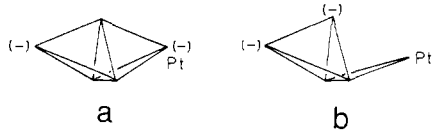

are five and span the equatorial metal triangle Pt–Ir1–Ir2 and the two opposite edges Ir1–Ir4 and Ir2–Ir3. This carbonyl disposition is the same as found in the isostructural dianion $[PtRh_4(CO)_{14}]^{2-}$.

The anion **2** is *not* isostructural with $[PtRh_4(CO)_{12}]^{2-}$ because of the lack, in the equatorial triangle, of the three coplanar bridging carbonyls, which are usually present in these trigonal bipyramidal structures; it shows, as a whole, idealized C_s symmetry, with a mirror plane passing through Pt, Ir2, and Ir4 and bisecting the Ir1–Ir3 edge. The nine terminal carbonyls are located one on platinum and two on each of the iridium atoms; the remaining three carbonyls bridge the apical–equatorial edges Pt–Ir1, Pt–Ir3, and Ir2–Ir4.

The ligand coordination around the apical metals in both anions is worth some consideration. In **1** the local geometry around the two Ir_{ap}, considering an additional ideal direction pointing toward the central M_3 triangle, is approximately that of a trigonal bipyramid. With reference to Ir3 in Figure 2, the almost colinear C5 and C13 can be considered the axial substituents, while the equatorial positions can be made coincident with C4, C6 and the direction pointing inside the cluster. The angles fit fairly well with this description: C5–Ir3–C13 = 170.0 (5)°, C4–Ir3–C6 = 123.5 (5)°, while C4–Ir3–C5, C5–Ir3–C6, C4–Ir3–C13, C6–Ir3–C13 are near enough to 90°. Similar considerations apply to the coordination around Ir4.

On the same basis, in compound **2** both the apical metals Pt and Ir4 can be considered in a square-planar environment, clearly recognizable in Figure 3. The maximum deviation from the least-squares plane of the pertinent atoms is ±0.15 Å and the angles C1B–Pt–C1, C1–Pt–C2B, C3B–Ir4–C42, and C42–Ir4–C41 (104.0 (3)°, 100 (4)°, 88 (4)°, and 92 (4)°, respectively) reasonably approximate the ideal situation. This situation, together with the above mentioned asymmetry of the M_{eq}–M_{ap} interactions where the CO bridged edges lying in the coordination plane are shorter than the unbridged and out of plane ones, suggests that the apical atoms can be seen as unsaturated centers. This is particularly true for the Pt atom for which the difference between the in-plane and out-of-plane Pt–Ir interactions is 0.3 Å. The cluster can consequently be seen as intermediate between the limiting cases *a* and *b*, sketched in Chart I. The anionic charges localized in *a* on the apical atoms give a limiting situation where all the metals attain a 18 VE configuration, while *b*, where one Pt–Ir bond loses and a charge moves on one equatorial Ir, has the Pt atom in a limiting 16 VE configuration.

Multinuclear NMR Studies. (a) $[PtIr_4(CO)_{14}]^{2-}$. Table IV reports ^{13}C NMR data obtained from ^{13}CO enriched samples of $[N\text{-}n\text{-}Bu_4]_2[PtIr_4(CO)_{14}]$ in THF-d_8 and $[PPN]_2[PtIr_4(CO)_{14}]$ (I) in acetone-d_6 at −97 °C; it can be seen that the shifts induced from different cations and/or solvents are usually less than 1 ppm. Variable temperature measurements (Table IV reports only the data of $[N\text{-}n\text{-}Bu_4]_2[PtIr_4(CO)_{14}]$) indicate that at low temperature the spectra (Figure 4) are consistent with an ideal C_2 symmetry,

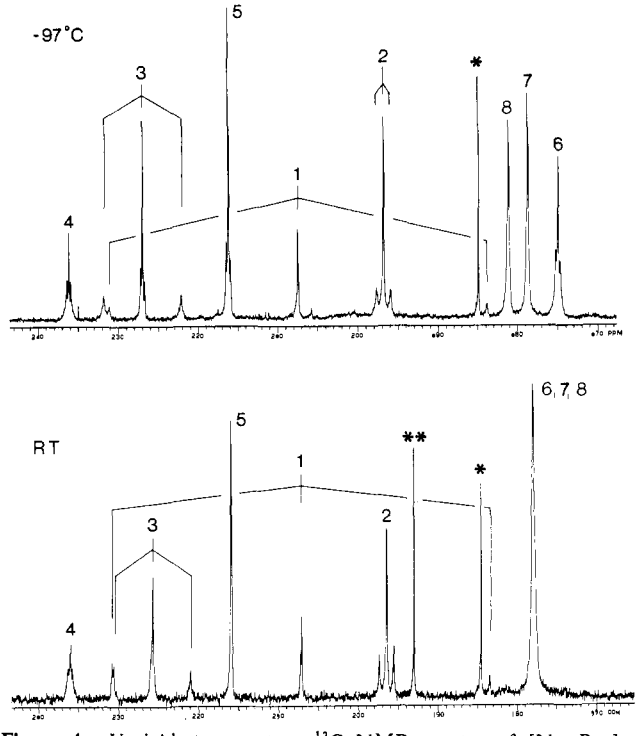

Figure 4. Variable-temperature ^{13}C NMR spectra of $[N\text{-}n\text{-}Bu_4]_2[PtIr_4(CO)_{14}]$ in THF-d_8 at −97 °C and room temperature. The resonances marked * and ** are impurities of $[Ir(CO)_4]^-$ and $[Ir_6(CO)_{15}]^{2-}$, respectively.

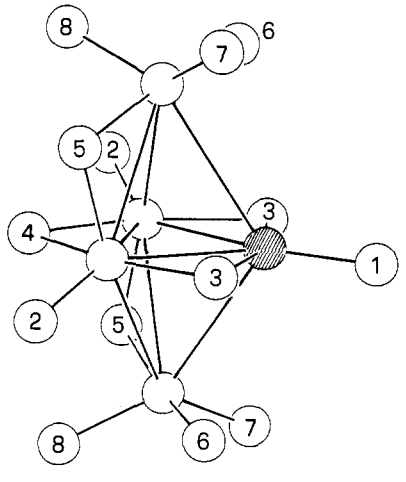

Figure 5. Schematic representation of the structure of $[PtIr_4(CO)_{14}]^{2-}$ with carbon labeling according to the C_2 symmetry. Dashed circle represents Pt atom.

the 2-fold axis incorporating C1, Pt, the center of the Ir_{eq}–Ir_{eq} edge, and C4, as depicted in the schematic structure of Figure 5. This geometry is the same as that previously found for $[PtRh_4(CO)_{14}]^{2-}$ (II), whose data at −105 °C[9] are also reported for comparison in Table IV.

The resonances due to the carbonyls C1–C4 lying in the equatorial plane are, as expected, of the relative intensities 1, 2, 2, and 1, respectively, and can be unambiguously assigned. Terminally bonded C1 (207.4 ppm) and C2 (196.7 ppm) are, as expected, at higher field than the bridging C3 (226.9 ppm) and C4 (236.0 ppm). $^1J_{Pt-C}$ = 2380 and 487 Hz, for C1 and C3, respectively, are comparable with those found for $[N\text{-}n\text{-}Bu_4]_2[PtRh_4(CO)_{14}]$ (II); two-bond Pt couplings, $^2J_{Pt-C2}$ = 87 Hz and $^2J_{Pt-C4}$ = 36 Hz,[19] were also observed. The larger value of the former is probably due to the nearly trans position of C2 with respect to Pt. The three high field resonances are assigned to the apical C6, C7, and C8 and that at 216.1 ppm to the bridging C5. It should be noted that, while no absolute assignment of C7 and C8 is possible, the resonance at 174.9 ppm can be unambiguously attributed to C6 because of a small coupling which is matched in the trans lying C5, $^2J_{C5-C6}$ = 27.6 Hz. Another two-bond C–C coupling has been seen, $^2J_{C3-C4}$ = ca. 25 Hz, this also deriving from a strong trans interaction.

Variable temperature ^{13}C spectra are invariant up to ca. −10 °C, when C6, C7, and C8 collapse while the coupling with C5 is lost. This can be explained by a rocking motion of the terminal carbonyls in the apical positions. At room temperature (Figure 4) C6, C7, and C8 are equivalent and give a single resonance at 177.9 ppm, in good agreement with the average value of 178.2 ppm which can be deduced from the data at −97 °C. All the other carbonyls appear static on the NMR time scale, and even $^2J_{C3-C4}$ can be seen.

Of particular note is the significant temperature dependent shift of C3 (1.2 ppm in the −97 °C to 25 °C range), particularly evident in the progressive movement of its low field satellite with respect to the low field satellite of C1.

Comparison with the data obtained for $[PtRh_4(CO)_{14}]^{2-}$ shows a shift of 10–30 ppm at lower frequencies of all the carbonyls bonded to iridium atoms. This is consistent with data obtained from isostructural compounds of Rh and Ir showing similar trends.[20] The platinum-bonded C1 is, on the contrary, shifted 14.2 ppm at higher frequencies; it is interesting to observe that the difference between the C1 chemical shift and the average of the other terminal carbonyls (C2, C6, C7, and C8) is −9.6 ppm in the case of $[PtRh_4(CO)_{14}]^{2-}$ and 24.6 ppm in the present case. C1 is now remarkably differentiated from the other terminal carbonyls, lying at the highest frequency very close to the region of bridging carbonyls.

^{195}Pt NMR of a ca. 20% ^{13}CO enriched sample of $[N\text{-}n\text{-}Bu_4]_2[PtIr_4(CO)_{14}]$ in acetone-d_6 at room temperature is shown in Figure 6a. The resonance found at −3723 ppm (reference to Na_2PtCl_6 in water) shows the expected pattern due to direct coupling with C1 and C3 and two-bond coupling with C2, $^1J_{Pt-C1}$ = 2383, $^1J_{Pt-C3}$ = 479, and $^2J_{Pt-C2}$ = 90 Hz (±3.5 Hz).

Finally it should be stressed that $[PtIr_4(CO)_{14}]^{2-}$ appears less fluxional than $[PtRh_4(CO)_{14}]^{2-}$. At a temperature as low as −75 °C, the latter shows scrambling of all the carbonyls C6, C7, C8, and even C5, in the upper and lower halves of the trigonal bipyramidal skeleton, while at room temperature only the equatorial bridging carbonyls C1, C3, and C4 stay fixed.

(b) $[PtIr_4(CO)_{12}]^{2-}$. We had some difficulty in obtaining NMR spectra of this species; this was mainly due to the preparation of reasonably pure, ^{13}CO enriched samples of salts sufficiently soluble at low temperature. Only at −103 °C, with the $[NMe\text{-}n\text{-}Bu_3]^+$ salt and very close to the freezing point of the solvent (see Experimental Section), we had evidence, through the broad band, ill-defined spectrum reported in Figure 7, of a "frozen" structure consistent with the idealized C_s symmetry previously discussed for $[PtIr_4(CO)_{12}]^{2-}$. The two signals in the bridging region, at 233.3 and 228.8 ppm and with relative intensities 1:2, can be unambiguously assigned (Figure 3) to the Ir_{ap}–Ir_{eq} bridging carbonyl 3B and to the Pt–Ir_{eq} bridging carbonyls 1B and 2B, respectively. The latter resonance shows the expected satellites due to Pt coupling, with $^1J_{Pt-C}$ = 611 Hz, typical of bridging carbonyls. The terminally bonded carbonyls give rise to resonances at 208.7, 203.9, 187.1, 185.5, 183.6, and 177.3 ppm, with approximate relative intensities of 1, 1, 2, 1, 2, and 2, respectively; this is consistent with the six groups of equivalent terminal COs recognizable under the C_s symmetry. Absolute assignments are, however, not possible, the exception being the resonance at 208.7 ppm: this is unambiguously due to the carbonyl terminally bonded on Pt because of the ^{195}Pt coupling ($^1J_{Pt-C}$ = 2320 Hz). This signal can be observed up to ca. −10 °C, whereas the remaining 11 carbonyls, at as low as −97 °C merge in a broad resonance centered at ca. 197 ppm. From −70 °C up to −10 °C (Figure 7) they appear divided in two groups, centered at ca. 197 and 195 ppm with relative intensities of ca. 9:2, respectively. The former resonance, in the −20 °C to −50 °C range, shows Pt satellites with a $^1J_{Pt-C}$ = ca. 165 Hz, indicative of a time-averaged short-range interaction with the Pt atom. It therefore appears reasonable to assign the resonance at 195 ppm to the two carbonyls terminally bonded on the apical Ir4. From −10 °C up to room temperature the fluxional process goes even further, and the resonance of the carbonyl terminally bonded on Pt is lost but without yet achieving the expected limiting condition of just one averaged resonance; the carbonyls now appear divided in two groups in an approximate ratio of 10:2.

^{195}Pt NMR of a 20–25% ^{13}C enriched sample at room temperature gives a broad ill-defined resonance at −3570 ppm, with J_{Pt-C} of ca. 200 Hz, not evident in the ^{13}C spectra. At −40 °C (Figure 6b) and −80 °C the resonances, at −3572 and −3590 respectively, are, as expected, a complex multiplet[21] with the recognizable time-averaged coupling of ca. 165 Hz together with the satellites due to $^1J_{Pt-C}$ = 2327 Hz, consistent with that observed in the ^{13}C resonance.

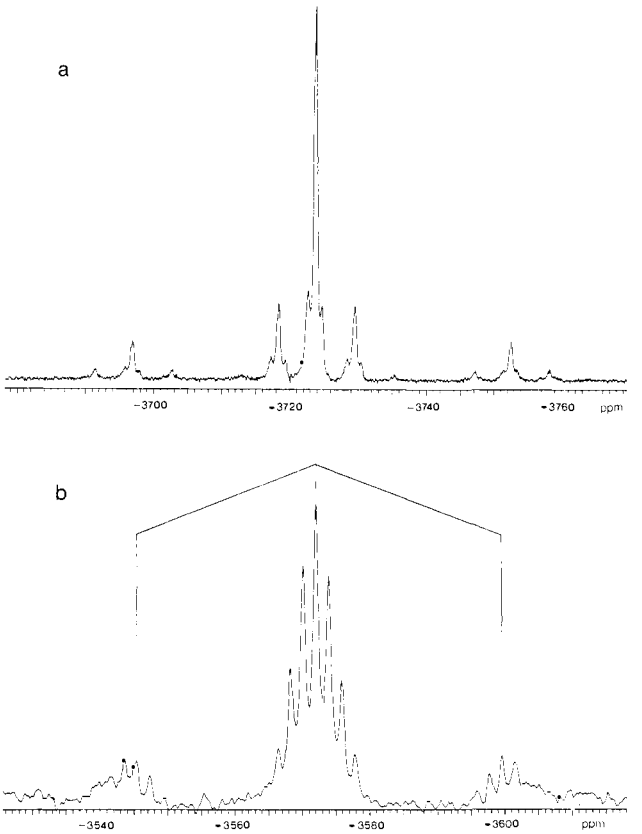

Figure 6. ^{195}Pt NMR in acetone-d_6 of the $[N\text{-}n\text{-}Bu_4]$ salts of (a) $[PtIr_4(CO)_{14}]^{2-}$ at room temperature and (b) $[PtIr_4(CO)_{12}]^{2-}$ at −40 °C, both ca. 20% ^{13}CO enriched.

Conclusions

The stabilization of the 72 CVE forms in $[PtIr_4(CO)_{12}]^{2-}$ and $[PtRh_4(CO)_{12}]^{2-}$, where the apical positions can be formally considered as electron deficient, appears to arise from the presence

(19) This coupling was detected only at −50 °C and at −10 °C in the $[PPN]_2[PtIr_4(CO)_{14}]$ complex.
(20) Fumagalli, A., unpublished results.

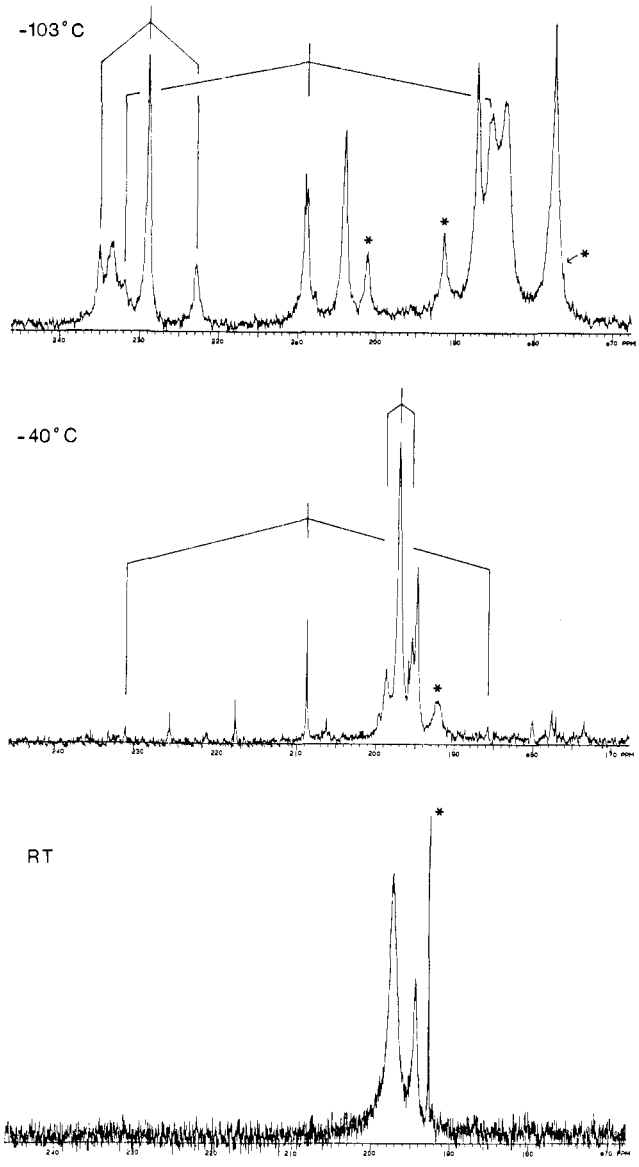

Figure 7. Variable-temperature ^{13}C NMR spectra of $[NMe\text{-}n\text{-}Bu_3]_2[PtIr_4(CO)_{12}]$ in the solvent mixture THF-d_8/$CHFCl_2$ (3:1, v:v), at −103 °C, −40 °C, and room temperature. The resonances marked * indicate an impurity of $[Ir_6(CO)_{15}]^{2-}$ which gives one resonance at room temperature and three of relative intensities 2:2:1 at low temperature. Small peaks at −40 °C are due to a small amount of $[PtIr_4(CO)_{14}]^{2-}$.

of both platinum and iridium (or rhodium) and ought therefore to be related to their aptitude for electron-deficient, square-planar structures. The stability of $Os_5(CO)_{16}$ and $[HOs_5(CO)_{15}]^-$ [2] with 72 CVEs appears, most likely, to be due to steric requirements which hinder a higher coordination of ligands to yield the formation of a 76 CVE species. This argument can explain the reaction of $Os_5(CO)_{16}$, which under CO pressure gives the open, and thus sterically relieved, "bow-tie" structure of $Os_5(CO)_{19}$.[22]

The difference of four electrons between the two forms is consistent with the picture of a cluster as a "sponge" of electrons, in that often relatively small skeletal changes induce a change of the CVMOs, as in our case where there is an elongation-contraction of the trigonal bipyramidal cage.[23,24]

Table V. X-ray Data for $[PPh_4]_2[PtIr_4(CO)_{14}]$ and $[NEt_4]_2[PtIr_4(CO)_{12}]$

formula	$PtIr_4P_2O_{14}C_{62}H_{40}$	$PtIr_4O_{12}N_2C_{28}H_{40}$
fw	2034.84	1560.53
cryst system	triclinic	orthorhombic
a, Å	13.868 (3)	15.453 (5)
b, Å	21.997 (5)	22.340 (5)
c, Å	10.804 (2)	33.422 (8)
α, deg	102.51 (2)	
β, deg	106.29 (2)	
γ, deg	98.02 (2)	
V, Å^3	3016.9	11537.9
Z, D_{calcd}, g/cm^3	2, 2.240	12, 2.695
space group	$P\bar{1}$ (n.2)	$Pnma$[a]
F(000)	1880	8448
μ(Mo Kα), cm^{-1}	112.1	183.4
2θ range, deg	6–50	6–44
scan method	ω	ω
scan interval, deg	0.9 + 0.347 tan θ	1.3 + 0.347 tan θ
prescan speed, deg min^{-1}	20	20
prescan acceptance $\sigma(I)/I$	1	1
required $\sigma(I)/I$	0.01	0.01
max time for one reflcn measd, s	70	45
collectd octants	$\pm h,\pm k,+l$	$+h,+k,+l$
no. of data collectd	10580	7612
no. of data used, $I > 3\sigma(I)$	6545	1579
cryst decay	27%	no decay
no. azimut reflcns for abs corr	3	3
max–min transmissn factor	1.00–0.61	1.00–0.32
R[c]	0.033	0.056
R_w[b,c]	0.039	0.057
no. of variable params	562	329
max peak in final diff Fourier (e Å^{-3})	1.20	1.49

[a] Nonstandard setting of *Pnam* n.62. [b] $w = 4F_o^2/\sigma(F_o^2)^2$ where $\sigma(F_o^2) = [\sigma(I)^2 + (pI)^2]^{1/2}/LP$. [c] $R = [\sum(F_o - k|F_c|)/\sum F_o]$; $R_w = [\sum w(F_o - k|F_c|)^2/\sum wF_o^2]^{1/2}$.

Alternatively we can see these molecules as containing two 16–18-electron centers. For this purpose, it is worth noting that, according to the work done by Dahl on the 76 CVEs clusters $[M_2Ni_3(CO)_{16}]^{2-}$ (M = Cr, Mo, W),[25] the apical groups, in our case the 14-electron $PtCO(\mu\text{-}CO)_2$ and $Ir(CO)_2(\mu\text{-}CO)$ in compound **2**, and the two 16-electron $Ir(CO)_3(\mu\text{-}CO)$ in compound **1** may be regarded as bonded to a cyclopropenyl-like M_3 ring system which occupies a fourth or fifth coordination site and acts as a two-electron donor. In this way the apical metals attain the formal 16- or 18-electron configuration with the proper square-planar or trigonal bipyramidal ligand geometry. In other words, the extension of the 16–18-electron rule[26] to the case of pentanuclear clusters could lead to a 72–76-electron rule.

Experimental Section

All the reactions and subsequent manipulations were carried out, unless otherwise specified, under nitrogen; the solvents were analytical grade and were distilled and stored under nitrogen. Na_2PtCl_6 was recrystallized and used in both the hexahydrated form and the anhydrous form obtained by vacuum drying at 100 °C; commercially available $IrCl_3$·ca. $3H_2O$ was used with ca. 52–53% Ir. $Ir_4(CO)_{12}$ was prepared according to the literature.[27]

^{13}C and ^{195}Pt NMR measurements were carried out at 50.3 and 42.86 MHz, respectively, on Varian or Bruker equipment; ^{195}Pt chemical shifts are in ppm (δ) down field from the external standard Na_2PtCl_6 in D_2O. ^{13}CO enriched samples (ca. 20–30%) were obtained by direct exchange at room temperature with 90% ^{13}CO, with standard vacuum-line techniques, on various salts of $[PtIr_4(CO)_{14}]^{2-}$; $[PtIr_4(CO)_{12}]^{2-}$ was obtained from the latter by vacuum removal of CO. The spectra were recorded under ca. 1 atm of pressure of ^{13}CO for $[PtIr_4(CO)_{14}]^{2-}$ and under N_2 for the other samples. In the low-temperature experiments, the solvent

(21) The complex multiplet is given by the superimposition of a singlet, a doublet, a triplet, a quartet... and so on, all with the same J and with relative intensities which can be deduced with a statistical calculation analogous to that reported in the following: Brown, C.; Heaton, B. T.; Towl, A. D. C.; Chini, P.; Fumagalli, A.; Longoni, G. *J. Organomet. Chem.* **1979**, *181*, 233.

(22) Farrar, D. H.; Johnson, B. F. G.; Lewis, J.; Nicholls, J. N.; Raithby, P. R.; Rosales, M. J. *J. Chem. Soc., Chem. Commun.* **1981**, 273.

(23) Lauher, J. W. *J. Am. Chem. Soc.* **1978**, *100*, 5305.

(24) Ciani, G.; Sironi, A. *J. Organomet. Chem.* **1980**, *197*, 233.

(25) Ruff, J. K.; White, R. P., Jr.; Dahl, L. F. *J. Am. Chem. Soc.* **1971**, *93*, 2159.

(26) Tolman, C. A. *Chem. Soc. Rev.* **1972**, *1*, 337.

(27) Della Pergola, R.; Garlaschelli, L.; Martinengo, S. *J. Organomet. Chem.* **1987**, *331*, 271.

Table VI. Positional Parameters for $[PPh_4]_2[PtIr_4(CO)_{14}]$

atom	x	y	z	atom	x	y	z
Pt	−0.25455 (3)	0.29830 (2)	−0.02636 (5)	C115	0.813 (1)	0.5360 (6)	0.095 (1)
Ir1	−0.06906 (3)	0.26842 (2)	0.05477 (4)	C116	0.7356 (8)	0.525 (5)	0.151 (1)
Ir2	−0.24381 (3)	0.18178 (2)	0.00955 (5)	C121	0.5599 (7)	0.4664 (4)	0.2517 (9)
Ir3	−0.19914 (3)	0.20084 (2)	−0.23592 (5)	C122	0.5764 (7)	0.4118 (5)	0.180 (1)
Ir4	−0.16857 (3)	0.28749 (2)	0.27028 (5)	C123	0.4959 (9)	0.3623 (5)	0.098 (1)
Ir5	−0.2482 (3)	0.1506 (2)	−0.1168 (5)	C124	0.3964 (9)	0.3684 (6)	0.085 (1)
Ir6	−0.1503 (3)	0.3232 (2)	0.1306 (4)	C125	0.3797 (9)	0.4241 (5)	0.154 (1)
Ir7	−0.0957 (3)	0.2554 (2)	−0.0747 (4)	C126	0.4588 (8)	0.4727 (5)	0.237 (1)
Ir8	−0.3005 (3)	0.2681 (2)	−0.1219 (4)	C131	0.6236 (7)	0.6007 (5)	0.408 (1)
Ir9	−0.1079 (3)	0.2067 (2)	0.1359 (4)	C132	0.6041 (9)	0.6188 (6)	0.526 (1)
Ir10	−0.3134 (3)	0.2176 (2)	0.0810 (4)	C133	0.568 (1)	0.6759 (7)	0.558 (1)
P1	0.6646 (2)	0.5272 (1)	0.3651 (3)	C134	0.554 (1)	0.7083 (6)	0.467 (1)
P2	0.2125 (2)	0.0994 (1)	0.4182 (3)	C135	0.570 (1)	0.6932 (6)	0.349 (1)
O1	−0.3653 (6)	0.3965 (3)	−0.1116 (8)	C136	0.6097 (9)	0.6373 (5)	0.321 (1)
O2	−0.3367 (9)	0.0815 (5)	0.116 (1)	C141	0.7143 (7)	0.5022 (4)	0.5133 (9)
O3	0.1409 (5)	0.2881 (4)	0.0312 (9)	C142	0.7914 (8)	0.5428 (5)	0.623 (1)
O4	−0.0369 (6)	0.1313 (4)	−0.301 (1)	C143	0.8349 (8)	0.5192 (5)	0.734 (1)
O5	−0.1098 (7)	0.3226 (4)	−0.2929 (9)	C144	0.8029 (9)	0.4611 (5)	0.732 (1)
O6	−0.4050 (8)	0.1803 (5)	−0.452 (1)	C145	0.7237 (9)	0.4187 (5)	0.622 (1)
O7	−0.1183 (8)	0.1897 (4)	0.4280 (9)	C146	0.6810 (7)	0.4394 (5)	0.514 (1)
O8	−0.3905 (6)	0.2637 (5)	0.262 (1)	C211	0.2718 (8)	0.1231 (5)	0.306 (1)
O9	−0.1167 (8)	0.4282 (4)	0.397 (1)	C212	0.365 (1)	0.1138 (9)	0.302 (2)
O10	−0.0681 (5)	0.4061 (3)	0.0236 (8)	C213	0.403 (2)	0.129 (1)	0.204 (2)
O11	−0.4636 (6)	0.2089 (4)	−0.0864 (9)	C214	0.361 (1)	0.1601 (7)	0.119 (1)
O12	−0.0373 (6)	0.1393 (3)	0.1068 (9)	C215	0.277 (1)	0.1761 (7)	0.138 (2)
O13	−0.2903 (6)	0.0703 (4)	−0.2204 (9)	C216	0.227 (1)	0.1573 (7)	0.222 (2)
O14	0.0626 (5)	0.3212 (3)	0.3336 (7)	C221	0.0903 (7)	0.0525 (5)	0.325 (1)
C1	−0.3257 (7)	0.3590 (5)	−0.081 (1)	C222	0.0062 (9)	0.0602 (6)	0.365 (1)
C2	−0.300 (1)	0.1173 (6)	0.075 (1)	C223	−0.092 (1)	0.0227 (7)	0.284 (1)
C3	0.0595 (8)	0.2785 (5)	0.035 (1)	C224	−0.100 (1)	−0.0198 (6)	0.172 (1)
C4	−0.0944 (8)	0.1555 (5)	−0.266 (1)	C225	−0.0232 (9)	−0.0296 (6)	0.129 (1)
C5	−0.1384 (9)	0.2801 (6)	−0.260 (1)	C226	0.0754 (9)	0.0076 (5)	0.207 (1)
C6	−0.3314 (9)	0.1885 (6)	−0.367 (1)	C231	0.2003 (8)	0.1667 (5)	0.533 (1)
C7	−0.1353 (9)	0.2237 (6)	0.368 (1)	C232	0.1603 (9)	0.2142 (5)	0.495 (1)
C8	−0.3155 (9)	0.2687 (6)	0.252 (1)	C233	0.142 (1)	0.2636 (6)	0.585 (1)
C9	−0.1414 (9)	0.3767 (5)	0.341 (1)	C234	0.162 (1)	0.2632 (6)	0.712 (1)
C10	−0.1026 (7)	0.3536 (5)	0.023 (1)	C235	0.205 (1)	0.2178 (8)	0.758 (2)
C11	−0.3756 (8)	0.2186 (5)	−0.058 (1)	C236	0.224 (1)	0.1688 (7)	0.665 (1)
C12	−0.0899 (8)	0.1723 (5)	0.071 (1)	C241	0.2916 (8)	0.0543 (5)	0.508 (1)
C13	−0.2583 (8)	0.1245 (5)	−0.176 (1)	C242	0.2563 (8)	−0.0060 (5)	0.501 (1)
C14	−0.0198 (8)	0.3008 (4)	0.2551 (9)	C243	0.3157 (9)	−0.0398 (6)	0.578 (1)
C111	0.7618 (7)	0.5383 (4)	0.288 (1)	C244	0.410 (1)	−0.0105 (7)	0.662 (1)
C112	0.8634 (8)	0.5614 (5)	0.363 (1)	C245	0.445 (2)	0.0522 (9)	0.676 (2)
C113	0.9372 (8)	0.5720 (5)	0.304 (1)	C246	0.380 (1)	0.0846 (9)	0.602 (2)
C114	0.9103 (9)	0.5583 (6)	0.169 (1)				

was a mixture, prepared at low temperature but stable at room temperature, of THF-d_8 and Genetron 21 ($CHFCl_2$) ca. 3:1 (v:v).

Infrared spectra were recorded on a Perkin-Elmer 781 grating spectrophotometer with 0.1 mm calcium fluoride cells previously purged with nitrogen or carbon monoxide.

(a) Synthesis of $[PPN]_2[PtIr_4(CO)_{14}]$ from $IrCl_3$ and Na_2PtCl_6. $IrCl_3$·ca. $3H_2O$ (53% Ir; 1.528 g, 4.21 mmol) and anhydrous Na_2PtCl_6 (0.478 g, 1.052 mmol) were placed in a two-necked, 500-mL, round-bottomed flask equipped with an inlet stopcock, a stopper, and a Teflon covered stirring magnetic bar; the large flask favors the exchange with the gaseous phase. Methanol (35 mL) was added, and the resulting solution, with some suspended material, was briefly evacuated and submitted to CO through a mercury valve maintaining a slightly positive pressure. A few minutes were required to saturate the solution with CO, then NaOH (2.1 M, 13.5 mL, 28.35 mmol) was added, and the mixture was stirred vigorously. The maximum CO absorption was observed within the first 2 or 3 h, and special attention was needed to avoid a decrease of the CO pressure. In about 24 h an orange-yellow solution was obtained with some precipitate, primarily NaCl and Na_2CO_3. The anion was precipitated by the addition of [PPN]Cl (2.280 g, 4 mmol in 20 mL methanol) and 20 more mL of water; the precipitate, as orange-yellow flakes or microcrystals, was separated from the mother liquor by filtration under CO, washed carefully with water (6 × 10 mL) and 2-propanol (4 × 10 mL), briefly dried in vacuum, and stored under CO. The product, checked by IR, showed a slight $[PPN][Ir(CO)_4]$ impurity so recrystallization was performed by slow diffusion of 2-propanol (40 mL), previously saturated with CO and cautiously layered on a solution of the product in THF (10 mL), under a CO atmosphere.

When the diffusion was completed, the crystalline precipitate was filtered, washed with 2-propanol (5 + 5 mL), vacuum dried, and stored under CO: yield 1.15 g (45%).

Anal. % found (% calcd) for $C_{86}H_{60}Ir_4N_2O_{14}P_4Pt$: C, 42.17 (42.45); H, 2.38 (2.49); N, 1.03 (1.15).

(b) Synthesis of $[N\text{-}n\text{-}Bu_4]_2[PtIr_4(CO)_{14}]$ from $Ir_4(CO)_{12}$ and Na_2PtCl_6. $Ir_4(CO)_{12}$ (1.489 g, 1.348 mmol) and anhydrous Na_2PtCl_6 (0.615 g, 1.356 mmol) were placed in a two-necked, 500-mL, round-bottomed flask equipped with an inlet stopcock, a stopper, and a Teflon covered stirring magnetic bar. Methanol (60 mL) was added, and the resulting suspension was briefly evacuated and submitted to CO through a mercury valve maintaining a slightly positive pressure. After about the 10 min which were required to saturate the solution with CO, NaOH in pellets (1.140 g, 28.5 mmol) was added, and the mixture was stirred vigorously. The maximum CO absorption was observed within the first 2 or 3 h, and special attention was needed to avoid a decrease of the CO pressure. In 20 h an orange-yellow solution was obtained with a white precipitate, primarily NaCl and Na_2CO_3. The solution was filtered under CO atmosphere, and the residue, before being discharged, was washed with MeOH (10 mL). The solution and collected washings were treated with $[N\text{-}n\text{Bu}_4]$Br (4.0 g in 8 mL MeOH) which caused partial precipitation; recovery was completed with the addition of water (20 mL). The yellow precipitate was filtered under CO and washed carefully with water (6 × 10 mL) and 2-propanol (15 mL). The product, during vacuum drying, changed color to orange-red but turned yellow when resubmitted to CO for storing. After the extraction of the product with THF (10 mL), recrystallization was performed under CO, by the slow diffusion of cautiously layered 2-propanol (40 mL). The yield of product, as beautiful yellow-orange crystals, was 1.532 g (62%).

Anal. % found (% calcd) for $C_{46}H_{72}Ir_4N_2O_{14}Pt$: C, 29.43 (30.01); H, 3.97 (3.94); N, 1.39 (1.52).

The product has also been obtined as the salt of several other cations such as $[N\text{-}n\text{Pr}_4]^+$, $[NEt_4]^+$, $[NMe\text{-}n\text{Bu}_3]^+$, $[PPh_4]^+$, and $[AsPh_4]^+$. The procedure is the same as reported in *a* and *b*, and precipitation occurs

Table VII. Positional Parameters ($\times 10^4$) for $[NEt_4]_2[PtIr_4(CO)_{12}]$

atom	x	y	z	atom	x	y	z
Pt	3876 (2)	1803 (1)	5961 (1)	O1A	1070 (99)	−892 (83)	2500 (0)
Ir1	2230 (2)	1396 (1)	5982 (1)	C11A	2102 (92)	1873 (93)	2041 (58)
Ir2	3398 (2)	516 (1)	6133 (1)	O11A	1381 (87)	2052 (60)	1942 (40)
Ir3	3382 (2)	1010 (1)	5392 (1)	C21A	3205 (53)	876 (40)	3370 (21)
Ir4	2009 (2)	228 (2)	5641 (1)	O21A	3033 (51)	1017 (38)	3699 (20)
C1B	4456 (41)	1454 (36)	5472 (25)	C22A	4725 (99)	119 (56)	2825 (78)
O1B	5232 (30)	1429 (21)	5353 (16)	O22A	4309 (80)	−531 (42)	3088 (46)
C2B	2942 (52)	1986 (37)	6270 (25)	C31A	4850 (92)	2271 (50)	2242 (42)
O2B	2694 (33)	2267 (23)	6561 (19)	O31A	5269 (92)	2718 (49)	2245 (46)
C3B	2790 (49)	−230 (34)	5990 (27)	Ir1′	2788 (22)	1216 (15)	2066 (12)
O3B	2869 (35)	−707 (26)	6153 (20)	Ir2′	3823 (28)	402 (21)	2500 (0)
C1	4647 (45)	2343 (31)	6149 (28)	N1	2018 (31)	9016 (21)	818 (16)
O1	5069 (39)	2747 (26)	6234 (22)	CT11	2893 (40)	9091 (34)	983 (28)
C11	1587 (61)	1873 (39)	5624 (29)	CT12	1779 (49)	9552 (31)	588 (29)
O11	1227 (36)	2238 (25)	5453 (19)	CT13	2000 (61)	8489 (32)	555 (26)
C12	1314 (50)	1152 (40)	6291 (26)	CT14	1399 (56)	8930 (46)	1148 (24)
O12	882 (37)	986 (27)	6542 (19)	CT15	3338 (47)	8525 (30)	1148 (25)
C21	3261 (46)	530 (36)	6671 (18)	CT16	817 (49)	9399 (45)	525 (36)
O21	3120 (40)	614 (29)	7007 (17)	CT17	2578 (63)	8501 (48)	180 (31)
C22	4515 (33)	275 (31)	6134 (24)	CT18	1293 (83)	9315 (51)	1527 (32)
O22	5242 (27)	155 (21)	6105 (16)	N2	357 (33)	2722 (28)	815 (19)
C31	3009 (50)	1477 (35)	4991 (21)	CT21	838 (75)	2185 (31)	691 (33)
O31	2684 (30)	1709 (22)	4724 (16)	CT22	606 (67)	2889 (66)	1224 (24)
C32	3763 (44)	337 (28)	5122 (23)	CT23	556 (96)	3218 (34)	541 (34)
O32	4005 (31)	−78 (22)	4950 (17)	CT24	−577 (35)	2595 (71)	802 (40)
C41	1383 (40)	605 (29)	5256 (20)	CT25	842 (63)	1593 (38)	927 (33)
O41	1052 (45)	900 (29)	4997 (20)	CT26	1550 (66)	2943 (46)	1079 (35)
C42	1328 (66)	−433 (37)	5617 (41)	CT27	48 (52)	3723 (38)	748 (30)
O42	928 (45)	−864 (28)	5603 (28)	CT28	−130 (99)	2502 (99)	394 (55)
PtA	2181 (4)	171 (3)	2500	N3	−1178 (87)	6926 (63)	2500
Ir1A	2404 (4)	1372 (3)	2500	CT31	−592 (99)	6408 (88)	2500
Ir2A	3585 (3)	691 (2)	2902 (2)	CT32	−670 (99)	7481 (86)	2500
Ir3A	4116 (4)	1731 (3)	2500	CT33	−1735 (85)	6906 (72)	2145 (10)
C1BA	4656 (96)	1252 (99)	2961 (34)	CT35	398 (99)	6500 (99)	2500
O1BA	5365 (69)	1108 (71)	3071 (54)	CT36	−1039 (99)	8170 (99)	2500
C2BA	1379 (60)	802 (81)	2500	N4	2396 (99)	3961 (99)	2500
O2BA	613 (48)	900 (62)	2500	CT41	3353 (99)	4227 (99)	2500
C1A	1646 (99)	−559 (66)	2500	CT45	3806 (99)	4807 (99)	2500

on the addition of an excess of the chosen cation and, if necessary, water to complete the recovery. The products obtained are generally of good purity, as can be checked by IR or more easily judged from the color, minimal amounts of the most recurrent impurity, $[Ir_6(CO)_{15}]^{2-}$, giving a darker, orange to brown, tone to the canary yellow color of the pure product.

Synthesis of $[PtIr_4(CO)_{12}]^{2-}$. The procedure here reported for the $[PPN]^+$ salt is general and can be used to obtain any other salt by using the corresponding salt of the parent compound. $[PPN]_2[PtIr_4(CO)_{14}]$ (0.418 g) was dissolved in THF (8 mL) under nitrogen atmosphere. The solution was slowly evaporated under vacuum, and the reddish-brown solid obtained was redissolved in THF (5 mL) and again evaporated slowly to a final volume of ca. 4 mL. An IR spectrum revealed complete conversion to $[PPN]_2[PtIr_4(CO)_{12}]$. Recovery was accomplished by cautious layering of 2-propanol (20 mL). When diffusion was complete, the crystalline precipitate was filtered, washed with 2-propanol (5 + 5 mL), vacuum dried, and stored under nitrogen: yield 0.380 g (93%). When larger amounts of products are worked up, more than one cycle of evaporation and redissolution may be necessary; in any case purity should be checked by IR. Recrystallization using the slow diffusion technique can also be performed from acetone/2-propanol.

Anal. % found (% calcd) for $C_{84}H_{60}Ir_4N_2O_{12}P_4Pt$: C, 42.33 (42.44); H, 2.57 (2.54); N, 1.08 (1.18).

Reaction of $[PtIr_4(CO)_{12}]^{2-}$ with CO. A THF or acetone solution of any salt of $[PtIr_4(CO)_{12}]^{2-}$ prepared under nitrogen is briefly evacuated and submitted to 1 atm of CO; within minutes the color turns orange from the original reddish-brown, and the IR taken under CO shows complete conversion to $[PtIr_4(CO)_{14}]^{2-}$.

Collection of Diffraction Data. Several crystalline samples with different cations of both **1** and **2** were found unsuitable for X-ray analysis, and eventually crystals of reasonable quality for the data collection were found, respectively, in the $[PPh_4]^+$ and $[NE_4]^+$ salts. A yellow prism of $[PPh_4]_2[PtIr_4(CO)_{14}]$ and a red one of $[NEt_4]_2[PtIr_4(CO)_{12}]$ of approximate dimensions 0.25 × 0.15 × 0.10 and 0.20 × 0.10 × 0.10 mm, respectively, were mounted on a glass fiber; diffraction data were collected on an Enraf-Nonius CAD-4 in the hemisphere $(\pm h,\pm k,+l)$ and in the octant $(+h,+k,+l)$, respectively, under the conditions specified in Table V. The two data sets were corrected for Lorentz polarization effects, for absorption, and for decay, when necessary.

Solution and Refinement of the Structure of 1. The structure was solved by the heavy atom method that allowed the location of a trigonal bipyramid of metal atoms. A subsequent difference Fourier map showed, besides the two phosphorus atoms, six other peaks defining an octahedron overlapping the trigonal bipyramid with peak-to-peak distances similar to those found in $[Ir_6(CO)_{15}]^{2-}$. Knowing this anion to be a recurrent impurity we decided to treat these peaks as Ir atoms with multiplicity 0.096 (as obtained by refinement), while the atoms belonging to the trigonal bipyramid were refined with a multiplicity of 0.904. The crystal thus consists of $[Ir_6(CO)_{15}]^{2-}$ (10%) and $[PtIr_4(CO)_{14}]^{2-}$ (90%) moieties occupying the holes in the $[PPh_4]^+$ packing. The carbonyl ligands of the $[PtIr_4(CO)_{14}]^{2-}$ anion were refined with anisotropic thermal parameters and a multiplicity of 0.904, and no attempt was made to locate the carbonyl ligands of the $[Ir_6(CO)_{15}]^{2-}$ dianion. The carbon atoms of the $[PPh_4]^+$ cations were refined isotropically with hydrogen atoms riding at 0.95 Å. The weighting scheme used in the least-squares refinements was $w = 4F_o^2/(\sigma(F_o^2))^2$ where $\sigma(F_o^2) = [\sigma(I)^2 + (0.030I)^2]^{1/2}/LP$. Final R and R_w are 0.033 and 0.039, respectively. The final atomic positional parameters are presented in Table VI. All the computations were performed with the Enraf-Nonius SDP structure determination package on a PDP 11/34 computer.

Solution and Refinement of the Structure of 2. The structure was solved by direct methods (MULTAN) and difference Fourier syntheses. There are two independent trigonal bipyramidal clusters, one is ordered in a general position while the other lies on a mirror plane. The latter is disordered at two different positions (0.89:0.11 as obtained by refinement of the heavy atoms multiplicity) which have in common the apical metal atoms but have staggered equatorial triangles. The structure is completed by four independent $[NEt_4]^+$ cations, two in the general position and two lying on mirror planes. The overall content of the cell is 12 anions and 24 cations. While the light atoms of the anion in the general position are reasonably well determined, those around the cluster in the special position were refined constraining the overall geometry to be similar to that of the moiety in the general position (using the DFIX option of the SHELX-76 package). However the refined U values of some atoms are high, and some cation atoms are missing. All the atoms, except for the metals, were refined by using isotropic thermal factors. The

weighting scheme used in the least-squares refinements was $w = 1.17/(\sigma(F_o)^2 + 0.0020F_o^2)$. Final R and R_w were 0.056 and 0.057, respectively. The final atomic positional parameters are presented in Table VII. All the computations were performed with the SHELX-76 package on an IBM 3083 computer.

Acknowledgment. We thank Prof. S. Martinengo for his interest in this work and M. Bonfà for recording the NMR spectra.

Registry No. **1**$[PPh_4]_2$, 117469-96-2; **1**$[PPN]_2$, 117469-97-3; **1**$[NnBu_4]_2$, 117469-98-4; **2**$[NEt_4]_2$, 117470-01-6; **2**$[PPN]_2$, 117470-00-5; Na_2PtCl_6, 16923-58-3; $Ir_4(CO)_{12}$, 18827-81-1; Ir, 7439-88-5; Pt, 7440-06-4; ^{195}Pt, 14191-88-9.

Supplementary Material Available: Tables of thermal parameters for $[PPh_4]_2[PtIr_4(CO)_{14}]$ (**1**) and for $[NEt_4]_2[PtIr_4(CO)_{12}]$ (**2**), hydrogen atoms coordinates for **1** (9 pages); tables of observed and calculated structure factor amplitudes for **1** and for **2** (54 pages). Ordering information is given on any current masthead page.

Lattice-Engineered Micromodulation of Intramolecular Electron-Transfer Rates in Trinuclear Mixed-Valence Iron Acetate Complexes

Ho G. Jang,[1] Steven J. Geib,[2] Yuki Kaneko,[3] Motohiro Nakano,[3] Michio Sorai,*[,3] Arnold L. Rheingold,*[,2] Bernard Montez,[1] and David N. Hendrickson*[,1]

Contribution from the School of Chemical Sciences, University of Illinois, Urbana, Illinois 61801, Department of Chemistry, University of Delaware, Newark, Delaware 19716, and the Chemical Thermodynamics Laboratory, Faculty of Sciences, Osaka University, Toyonaka, Osaka 560, Japan. *Received June 16, 1988*

Abstract: The factors influencing the rate of intramolecular electron transfer in the solid state have been investigated for the oxo-centered, mixed-valence complexes $[Fe_3O(O_2CCH_3)_6(4\text{-Me-py})_3]S$, where S is either $CHCl_3$ (**1**), CH_3CCl_3 (**2**), CH_3CHCl_2 (**3**), or C_6H_6 (**4**), and $[Fe_3O(O_2CCH_3)_6(py)_3]S$, where S is either $CHCl_3$ (**5**) or C_5H_5N (**6**). Complex **1** crystallizes in the rhombohedral space group $R32$ with three molecules in a unit cell with dimensions $a = 18.759$ (6) Å, and $c = 10.373$ (3) Å at 298 K. The final discrepancy factors are $R = 0.0323$ and $R_w = 0.0363$ for 1166 reflections with $F_o > 5\sigma(F_o)$. The bond distances about each iron atom are Fe-O(oxide) = 1.912 (1) Å, Fe-N = 2.221 (4) Å and an average Fe-O(acetate) distance of 2.080 Å. Along the c-axis of complex **1**, Fe_3O complexes and $CHCl_3$ solvate molecules occupy alternating sites of 32 symmetry. The $CHCl_3$ solvate molecule is disordered about the three C_2 axes which are perpendicular to the C_3 axis. This disorder was modeled with the three Cl atoms in a plane, above and below which the C-H moiety was disordered with the C-H vector along the C_3 axis. Examination of the parameters (thermal and distances) resulting from this fit clearly indicates that the C-H vector of the $CHCl_3$ solvate is not just sitting on the C_3 axis but is also jumping to positions off the C_3 axis. Complex **5** also crystallizes in the $R32$ space group with $Z = 3$, $a = 17.819$ (6) Å, and $c = 10.488$ (3) Å at 298 K [$R = 0.0327$ and $R_w = 0.0377$ for 1373 reflections with $F_o > 5\sigma(F_o)$]. The $CHCl_3$ solvate molecules in **5** are disordered the same way as those in **1**. Substantiation for the onset of dynamic disorder of the $CHCl_3$ solvate molecules comes from heat capacity data measured for complex **5** between 14 and 300 K. A phase transition with two peaks closely centered at 207.14 and 208.19 K was found. The total transition enthalpy and entropy gain for the phase transition are $\Delta H = (5107 \pm 44)$ J mol^{-1} and $\Delta S = (28.10 \pm 0.44)$ JK^{-1} mol^{-1}. The entropy gain first appears at ~100 K as the temperature is increased from 14 K. The experimental ΔS can be accounted for by a combination of Fe_3O complexes converting from valence trapped in one vibronic state to dynamically converting between all four vibronic states ($\Delta S = R\ln 4$) and each of the $CHCl_3$ molecules going from static to dynamically jumping between eight positions ($\Delta S = R\ln 8$). The total $\Delta S = R\ln 32$ (= 28.82 JK^{-1} mol^{-1}) agrees with the experimental entropy gain. Variable temperature ^{57}Fe Mössbauer data are presented for all six complexes. In general, a valence-trapped spectrum with Fe^{II} and Fe^{III} doublets is seen at low temperatures. As the temperature is increased, a third doublet characteristic of an undistorted (delocalized) complex appears. Further increase in temperature changes the spectrum at a higher temperature to only a single doublet for delocalized complexes. The two temperatures for these occurrences are seen to be ~160 and ~208 K for complex **5**; the latter temperature agrees with the culmination temperature seen in the C_p data for the phase transition of complex **5**. The Mössbauer spectrum of complex **1** changes fairly abruptly with the third doublet first seen at ~81 K and the complete conversion to Mössbauer detrapped at ~90-95 K. This agrees with the DTA data for this complex which shows a peak at 95 K. It is interesting that complex **3** with its less symmetric CH_3CHCl_2 solvate molecule becomes valence detrapped on the Mössbauer time scale at 45° higher temperature than for the CH_3CCl_3 solvate **2**. A magnetically oriented sample of 20 small crystals of $CDCl_3$ solvate **5** in a wax block was employed with solid-state ^2H NMR spectroscopy to probe the dynamics of the chloroform solvate molecule. With the magnetic field directed down the c-axis the quadrupole splitting of the single ^2H NMR doublet remained relatively constant (196-204 kHz) in the range 295-208 K and then decreased below the phase transition temperature at 208 K to become eventually 144 kHz at 110 K. Above 208 K the $CDCl_3$ solvate molecule is jumping between eight positions, four with the C-D vector pointed up and four down, where for the four up positions one C-D vector position is along the c-axis and the other three are at an angle of 24.7° relative to the c-axis. At 110 K the C-D vector is static and takes only one position at an angle of 31.5° from the c-axis. The nature of the phase transitions seen for each of the **1-6** complexes is discussed. Intermolecular pyridine-pyridine ligand overlaps appear to be important in determining where the phase transition from a valence-trapped to a valence-detrapped state occurs. The solvate molecules, one above and one below each Fe_3O complex, also likely affect the rate of intramolecular electron transfer in each Fe_3O complex as the solvate molecules go from static to dynamic. The experimental results in this paper are compared to the predictions of a theoretical model based on a molecular field calculation.

Variations in environmental conditions can dramatically affect electron-transfer processes in chemical and biological systems.[4] It is not known, for example, what influence the dynamics of water and/or amino acid groups which comprise an electron-transfer

0002-7863/89/1511-0173$01.50/0